Journal of Medical Imaging

MedicalImaging.SPIEDigitalLibrary.org

Automatic quantification of *HER2* gene amplification in invasive breast cancer from chromogenic *in situ* hybridization whole slide images

Md. Shakhawat Hossain
Matthew G. Hanna
Naohiro Uraoka
Tomoya Nakamura
Marcia Edelweiss
Edi Brogi
Meera R. Hameed
Masahiro Yamaguchi
Dara S. Ross
Yukako Yagi

SPIE.

Md. Shakhawat Hossain, Matthew G. Hanna, Naohiro Uraoka, Tomoya Nakamura, Marcia Edelweiss, Edi Brogi, Meera R. Hameed, Masahiro Yamaguchi, Dara S. Ross, Yukako Yagi, "Automatic quantification of *HER2* gene amplification in invasive breast cancer from chromogenic *in situ* hybridization whole slide images," *J. Med. Imag.* **6**(4), 047501 (2019), doi: 10.1117/1.JMI.6.4.047501.

Automatic quantification of *HER2* gene amplification in invasive breast cancer from chromogenic *in situ* hybridization whole slide images

Md. Shakhawat Hossain,[a,b,*] Matthew G. Hanna,[b] Naohiro Uraoka,[b] Tomoya Nakamura,[a,c] Marcia Edelweiss,[b] Edi Brogi,[b] Meera R. Hameed,[b] Masahiro Yamaguchi,[a] Dara S. Ross,[b] and Yukako Yagi[b]
[a]Tokyo Institute of Technology, School of Engineering, Department of Information and Communications Engineering, Yokohama, Japan
[b]Memorial Sloan Kettering Cancer Center, Department of Pathology, New York, New York, United States
[c]Japan Science and Technology Agency, PRESTO, Saitama, Japan

Abstract. Human epidermal growth factor receptor 2 (HER2), a transmembrane tyrosine kinase receptor encoded by the *ERBB2* gene on chromosome 17q12, is a predictive and prognostic biomarker in invasive breast cancer (BC). Approximately 20% of BC are HER2-positive as a result of *ERBB2* gene amplification and overexpression of the HER2 protein. Quantification of *HER2* is performed routinely on all invasive BCs, to assist in clinical decision making for prognosis and treatment for *HER2*-positive BC patients by manually counting gene signals. We propose an automated system to quantify the *HER2* gene status from chromogenic *in situ* hybridization (CISH) whole slide images (WSI) in invasive BC. The proposed method selects untruncated and nonoverlapped singular nuclei from the cancer regions using color unmixing and machine learning techniques. Then, *HER2* and chromosome enumeration probe 17 (CEP17) signals are detected based on the RGB intensity and counted per nucleus. Finally, the *HER2*-to-CEP17 signal ratio is calculated to determine the *HER2* amplification status following the ASCO/CAP 2018 guidelines. The proposed method reduced the labor and time for the quantification. In the experiment, the correlation coefficient between the proposed automatic CISH quantification method and pathologist manual enumeration was 0.98. The *p*-values larger than 0.05 from the one-sided paired *t*-test ensured that the proposed method yields statistically indifferent results to the reference method. The method was established on WSI scanned by two different scanners. Through the experiments, the capability of the proposed system has been demonstrated. [DOI: 10.1117/1.JMI.6.4.047501]

Keywords: automatic CISH quantification; HER2-positive breast cancer; HER2 gene amplification; digital pathology; whole slide imaging.

Paper 19133SSRR received Jun. 4, 2019; accepted for publication Oct. 28, 2019; published online Nov. 21, 2019.

1 Introduction

Up to 20% of invasive breast cancers (BC) show human epidermal growth factor receptor 2 (*HER2*)/*ERBB2* gene amplification and subsequent HER2 protein overexpression.[1] The *HER2* amplification status in BC is a strong prognostic and predictive biomarker. *HER2* assessment is required to determine *HER2* amplification status in order to provide *HER2*-targeted therapy for this subset of patients with invasive BC.

In routine clinical practice, the traditional methods of assessment for *HER2* amplification status in BC include immunohistochemistry (IHC), fluorescence *in situ* hybridization (FISH), and bright-field dual-color chromogenic *in situ* hybridization (CISH). These are the FDA (U.S. Food and Drug Administration) approved methods for the assessment of *HER2* gene amplification in breast and gastric cancer. IHC detects the expression of the HER2 protein while *in situ* hybridization detects amplification of the *HER2* gene. IHC is reported according to the ASCO/CAP guidelines as negative (scores 0 and 1+), equivocal (score 2+), and positive (score 3+).

If IHC is equivocal, then reflex testing by FISH or CISH is required according to the ASCO/CAP guidelines.[2] FISH and CISH are quantitative methods, assessing the number of *HER2* and chromosome enumeration probe 17 (CEP17) copies per nucleus. FISH uses fluorescence microscopy, and methods are reported for manual, semiautomatic, and automatic quantification for *HER2* scoring using FISH images.[3–8] The automatic image analysis methods for FISH, proposed by Konsti et al. and Furrer et al.,[6,7] exhibit high concordance with manual FISH analysis, but the cost and turnaround time were not investigated. FISH requires special training, special probes, and is more expensive compared to IHC. In contrast, CISH uses bright-field microscopy, and CISH dyes are significantly less expensive than the fluorescence dye,[9,10] more comparable to an IHC test. In addition, CISH allows simultaneous assessment of morphology and gene copy number on the same slide and easier identification of tumor heterogeneity using low-level magnification. Since FISH probe signals will fade over time, archiving slides and referring to prior FISH studies are difficult, while CISH-stained slides fade at a much slower rate and can be archived similar to IHC slides. One disadvantage of CISH was reported, that it exhibits lower sensitivity for lower level amplifications.[10] The assessment was performed under a microscope. CISH assessment is performed by counting myriads of signals

*Address all correspondence to Md. Shakhawat Hossain, E-mail: shakhawat.h.aa@m.titech.ac.jp

2329-4302/2019/$28.00 © 2019 SPIE

manually under the microscope, which is time-prohibitive and laborious. Therefore, assessing CISH images and automatically quantifying the *HER2* and CEP17 signals to render an amplification status would be of great value, especially in large volume institutions. However, no such method has been reported for the automatic CISH assessment. Some commercial products exist for automatic CISH assessment. However, in our preliminary study, they failed to detect singular nuclei and quantify nuclei exhibiting overlapped regions and missing parts. Such an assessment is not reliable.

In this paper, we propose a system to quantify CISH whole slide images (WSI), to facilitate the automated determination of the *HER2* amplification status. The proposed method uses digital imaging analysis techniques and detects tumor nuclei, *HER2*, and CEP17 signals from the invasive cancer region of interest. A support vector machine (SVM) is used to select untruncated and nonoverlapped singular nuclei from the candidates. Then, *HER2* and CEP17 signals are segmented and counted for each nucleus. The proposed method follows the 2018 ASCO/CAP guidelines and quantified at least 20 nuclei per case with the highest *HER2*-CEP17 differential values to identify the amplification status. We developed an in-house application using the proposed method and are validating the proposed method at Memorial Sloan Kettering Cancer Center. While existing technology fails to detect isolated nuclei and quantify overlapped and partly missing nuclei, the proposed method successfully achieves the automation of CISH quantification by selecting the limited number of nuclei suitable for *HER2* and CEP17 signal evaluation, as the guideline suggests the minimum number of nuclei required for the quantification.

We performed CISH quantification for 22 BC patients using the proposed system and compared the quantification results with a subspecialized breast pathologist's interpreted IHC, manual FISH, and CISH scores. The results of our experiments ensured the effectiveness of the proposed system for automatic quantification of *HER2* gene amplification using CISH WSI. Further, we have estimated the time requirements.

2 Methods and Materials

2.1 *System Overview*

The proposed system uses high-resolution (e.g., 0.13 μm/pixel) CISH WSI and relies on the pathologist for invasive tumor annotation on a digital H&E slide to perform the automatic quantification. High-resolution image is required to observe the HER2 and CEP17 signals. Figure 1 shows the structure of the proposed system to determine the *HER2* gene amplification status. First, tissue blocks with a tumor are sectioned using an automatic sectioning machine, and 4 μm serial sections are produced for subsequent H&E and CISH staining. Then, the serial sections are stained in the automatic staining machine to prepare the H&E and CISH glass slides. We subsequently scan the H&E and CISH glass slides using the WSI scanner at 40× magnification to produce the WSI. Two subspecialized breast pathologists annotated the invasive cancer regions of interest (ROI) on the H&E WSI.

We exported the annotations from the H&E images to the CISH WSI of the serial section, in which the image registration is applied using 3DHISTECH's WSI viewer software. No manual parameters were used for image registration.

Then, the proposed method detects singular nuclei, *HER2* (black), and CEP17 (magenta) *in situ* hybridization signals from the annotated ROI. Signals are then counted per nucleus where CEP17 ≥ 2. The proposed method selects at least 20 nuclei with the highest HER2-CEP17 differentiation values. Then, the total *HER2* and total CEP17 signal counts are calculated for the selected nuclei. Finally, the *HER2* amplification status is determined as "positive" or "negative" as per the 2018 ASCO/CAP guidelines. If the number of *HER2* copies per nucleus falls into a *HER2* status category requiring an additional 20 nuclei to be counted, the model would additionally ensure that another set of at least 20 nuclei are similarly quantified. After that, the amplification status is determined based on the calculated *HER2* to CEP17 ratio and the average number of *HER2* copies per cell from at least 40 nuclei. Figure 2 shows the flowchart of the proposed method.

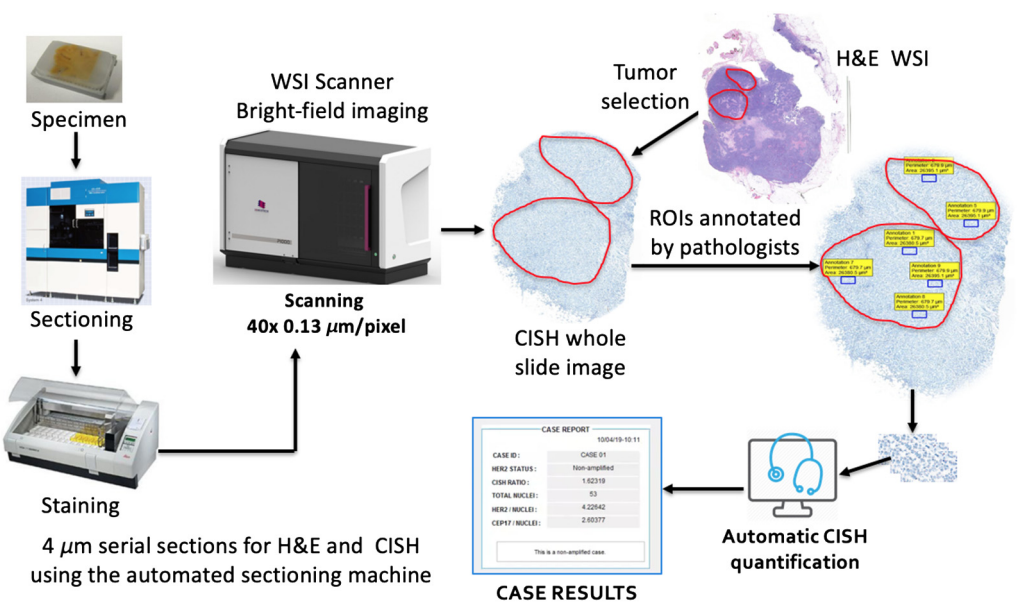

Fig. 1 Workflow for the proposed system.

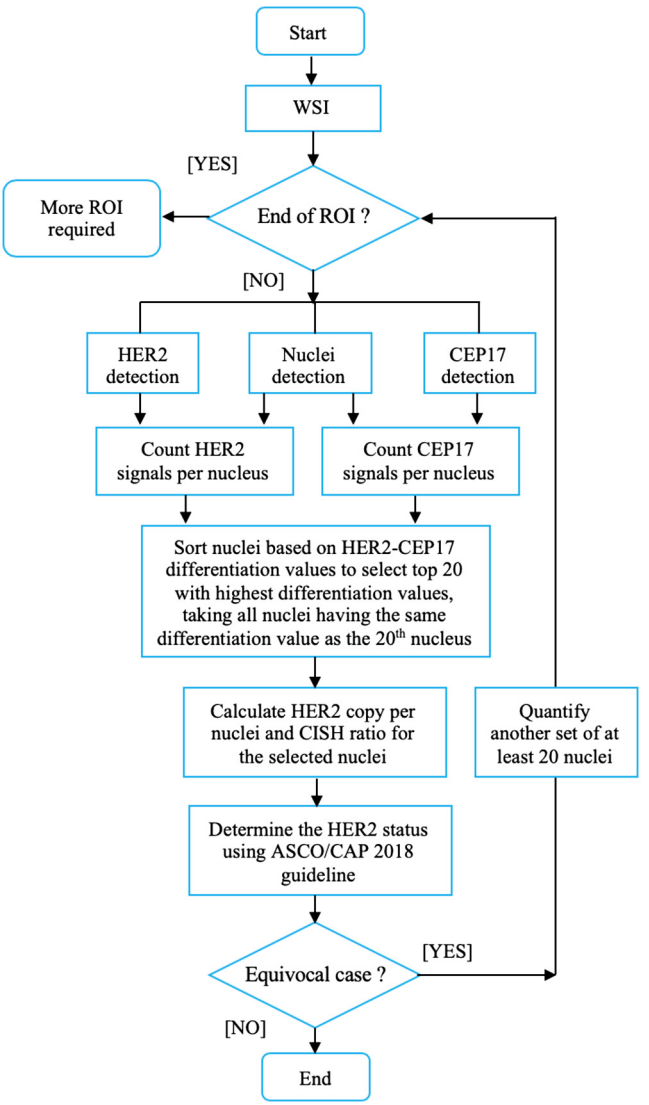

Fig. 2 Flowchart of the proposed method.

In our experiment, the CISH specimens were prepared using the VENTANA Ultra Red ISH DIG detection kit for *HER2* gene amplification. The INFORM HER2 dual ISH DNA probe cocktail probe was used, and the hybridization time was 6 h. The tissue was 4 μm thick as recommended by VENTANA.

2.2 *Nuclei Detection*

In the proposed method, at least 20 nuclei will be used for the assessment. As there are much more nuclei in the selected tissue, selecting the nuclei that are suitable for the quantification is necessary. For example, the nucleus that contains overlapped regions or partially missing regions need to be discarded. Moreover, existing methods for nuclear detection often produce false detection, which must not be included in the quantification. Therefore, for the robust and accurate quantification, the nuclear detection method consists of two stages: the candidate detection stage and the selection stage based on machine learning.

The first stage for detecting nuclei candidates consists of three phases: (1) background separation, (2) outliers' removal, and (3) partitioning. In (1) background separation, the proposed method uses the color unmixing technique[11,12] to separate the background from the nuclei regions. In CISH slides, HER2, CEP17, and nuclei become black, magenta, and blue, respectively. In color unmixing, the optical density values are derived from the RGB intensities of the original image using the log transform based on Beer–Lambert's law. The mathematical model used in color unmixing is given as

$$g_k = \log\left(\frac{I_{0\,k}}{I_k}\right), \qquad k = \mathrm{R}, \mathrm{G}, \mathrm{B}, \tag{1}$$

where $\mathbf{g} = (g_R\, g_G\, g_B)^t$ and $(I_R\, I_G\, I_B)^t$ are the optical density and the intensity of RGB components of every pixel, respectively. $(I_{0\,R}\, I_{0G}\, I_{0B})^t$ is the average intensity of glass pixels.

We estimated the average intensity for each channel of RGB for CEP17 and nuclei areas from multiple images. The samples included both normal and cancer cells. However, this is not going to impact on the signal and nuclei detection. The color unmixing technique derives in Eq. (1) resulting in three stain-separated grayscale images, one belongs to nuclei areas, one for the CEP17 areas, and the last as a leftover, shown in Fig. 3. For nuclear detection, the image of nuclei areas is used in the following steps.

After separating the background, the noise removal phase is invoked to suppress the non-nuclei pixels, which are the low-intensity pixels outside the nucleus. The outliers or noise removal is applied to the grayscale abundance image of nuclei. We assume the pixels exhibiting low-intensity and accompanied by low-intensity neighbors as noise. For nuclei detection, the noise is suppressed in three steps as the following, shown in Fig. 4.

1. Apply Otsu's 5-level adaptive thresholding on the image and the second lowest threshold is considered the status.
2. Pixels are classified as poor if intensity $\leq$ status or rich if intensity $>$ status.
3. A 5×5 filter is applied to every poor pixel, and its intensity is updated as:
   a. if the poor is accompanied by more than four rich neighbors then intensity is kept unchanged,
   b. otherwise replace with zero.

The next step is partitioning, which is implemented using commonly used morphological operations. Before the partitioning process, a morphological opening is used to remove small objects. Then, the noise removed image is converted into a binary image, and the outer boundary of each object is detected to partition slightly jointed nucleus, and the holes of each object are filled.

Distance transformation and watershed technique are used to separate the nuclei that slightly jointed (one nucleus touching the boundary of another) and those that are overlapped.[13] At first, the distance transformation is applied to the complemented binary image. Then, the resultant image is complemented again, and watershed technique was applied to split nuclei along the watershed lines. Figure 5 shows the partitioning of slightly jointed nuclei.

After removing very small and large objects where the partitioning fails, the rest of the objects are considered as candidates, and machine learning is used to detect the singular nuclei.

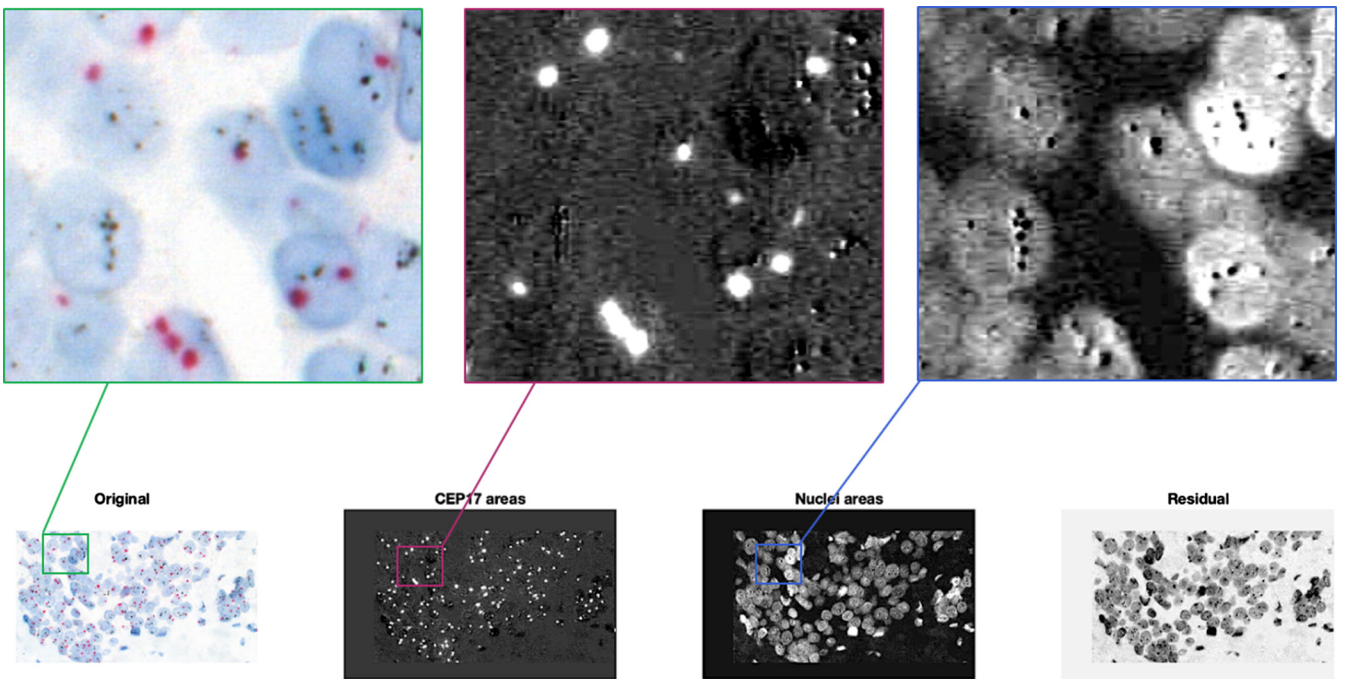

Fig. 3 Background separation for nuclei and CEP17 detection using color unmixing.

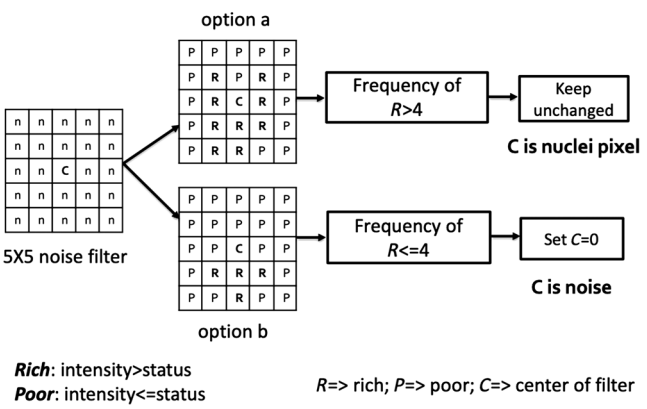

Fig. 4 5 × 5 filter to remove noise for nuclei detection.

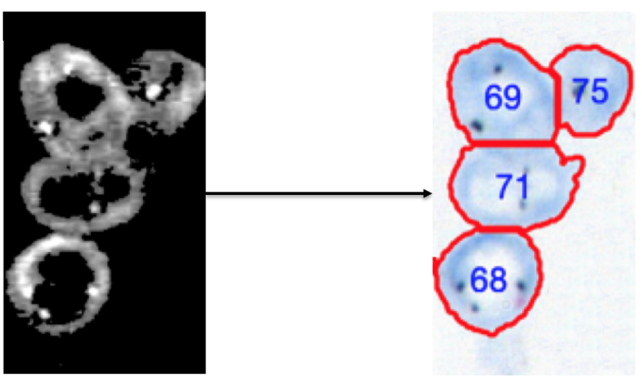

Fig. 5 Partitioning slightly jointed nuclei mesh using distance transformation and watershed.

Since the candidate nuclei detected up to this stage may include those that exhibit missing parts or contained some overlapped regions, an image classification technique based on machine learning is used to select singular nuclei and eliminate overlapped and truncated nuclei. A nonlinear SVM binary classifier is applied to select singular nuclei using nine shape and boundary-based features.[14–16] SVM classifier was selected as it can work effectively on a smaller dataset. The list of nine features and their formula are presented in Sec. 6 Appendix A.

To determine those features, we conducted the preliminary experiment as follows. Initially, we selected 21 shape and boundary descriptor features as candidates. Then, the nine most prominent features were selected among them using the sequential feature selection method.[17] The sequential feature selection used a 10-fold cross-validation. The 10-fold cross-validation was performed using 3020 nuclei, extracted from 15 different cancer regions belonging to seven WSI, each from a different patient case. Features were ranked based on the resultant of the classification error rate when added to the existing feature set. Primarily, we selected the first 11 features when the classification reached a stable point. The error rate started increasing with the inclusion of the 12th feature and afterward. Table 1 shows the results of the sequential feature selection experiment. Finally, we decided on the nine features from the 11 primarily selected features and rejected two of them. Eccentricity and compactness were rejected as they produce similar measurements such as elongation and roundness accordingly but exhibit lower significance.

Later, to ensure the accuracy of the SVM classifier to select singular nuclei, we tested the classifier to select singular nuclei from a different dataset. The average classification accuracy was found above 90% in the 4-fold cross-validation. The output of the SVM for each candidate nucleus is a score, which is the probability provided by the SVM classifier. A higher score indicates more accurate detection for a nucleus. Then, for the purpose to quantify at least 20 nuclei per case, we select nuclei with the top 20 highest scores, which are suitable for the quantification.

Table 1 List of candidate features with the rank.

Candidate features	Error rate	Rank	Remarks
Roundness	0.2139	1	Selected
Area_to_peri	0.1274	2	Selected
Std_cen_to_boundary	0.115	3	Selected
Curl	0.1118	4	Selected
Elongation	0.1109	5	Selected
Eccentricity	0.1097	6	Rejected: similar measure as elongation
Extent	0.109	7	Selected
Compactness	0.1087	8	Rejected: similar measure as roundness
Solidity	0.1085	9	Selected
Convexity	0.1089	10	Selected
Avg_bend_energy	0.1087	11	Selected
EquivDiameter	0.1218	12	Rejected
Minor axis length	0.1521	13	Rejected
Major axis length	0.2007	14	Rejected
Perimeter	0.4196	15	Rejected
Sum of the gradient of curvature	0.4745	16	Rejected
Total absolute curvature	0.4823	17	Rejected
Area-to-total curvature ratio	0.4844	18	Rejected
Area	0.4854	19	Rejected
Difference between convex area and area	0.4854	20	Rejected
Sum of distances from centroid to boundary	0.4854	21	Rejected

2.3 *CEP17 Detection and Counting*

The CEP17 signal detection process consists of four steps: (1) the background separation, (2) the outliers removal, (3) separation of jointed signals, and (4) scoring. The steps to detect and count CEP17 signals are described in the following. Figure 6 shows the signal (CEP17 and *HER2*) detection approach in common. The proposed system detects signals from the entire area for a given input and keeps a list of signals. Then, the signals are counted for a selected nucleus if it falls inside the nucleus boundary after nuclei detection.

In the first step, the background is separated by the color unmixing technique, which is described in Sec. 2.2. The abundance image of CEP17, obtained by color unmixing is used in the following steps. We applied Otsu's five-level thresholding on the grayscale abundance image to remove pixels with low

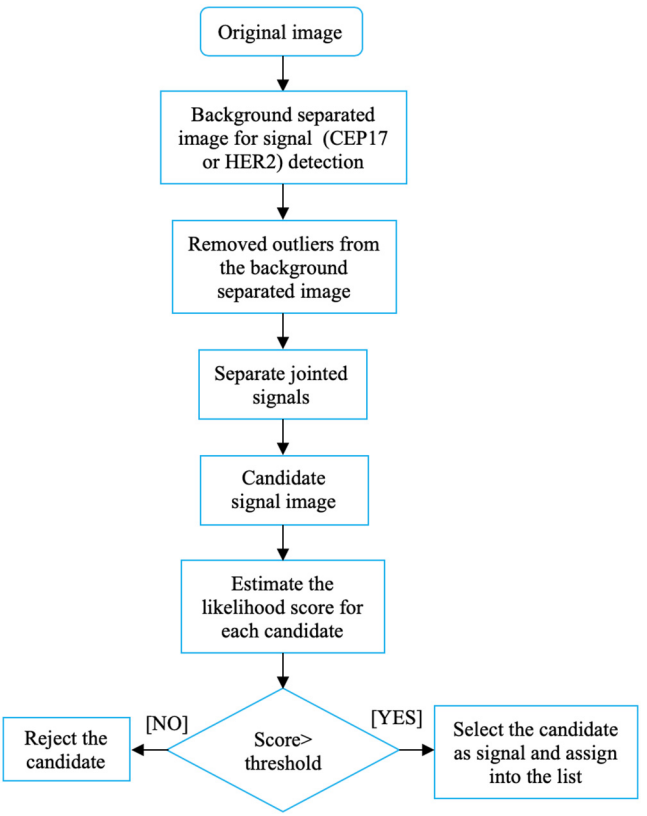

Fig. 6 Flowchart for detecting and counting signals (CEP17 and *HER2*).

abundance, which is smaller than the highest threshold. A binary image is created by converting the low abundance pixels to zero and high abundance pixels to one.

The next step is to remove outliers. We ignored weak signals and considered only the pure ones for quantification. Thus, the proposed method rejected overlapped signals. First, the binary image is used as a mask to retrieve the color image, and then two different types of noises are removed from it. We assumed that pixels with high intensity in all channels of RGB belong to glass area and removed them as noise. In CISH images, originally CEP17 signals appear as magenta, but the color changes when overlapped by black HER2 dye or blue nuclei dye. Such pixels are considered as noise and removed based on the hue value of HSV color space. We eliminated a pixel if the hue angle lies between 50 deg and 240 deg.

After removing the noise, jointed signals are partitioned using the distance transformation followed by the watershed algorithm, shown in Fig. 7. We assume that the size of CEP17 signals follows normal distribution and considered only those signals that fall within two standard deviations. After partitioning the jointed signals, a region with an area smaller than 10 pixels and larger than 350 pixels is eliminated. After that, each segmented region is labeled and considered to be a candidate region of CEP17 signal.

In fact, the candidate regions obtained by the above process contain weak signals. The proposed method ignores weak signals and counts only strong signals for quantification. To remove the weak signals, each candidate region is scored based on the probability of the CEP17 signal using an RGB intensity of pixels. If the score is larger than a certain threshold, the region is concluded as a CEP17 signal.

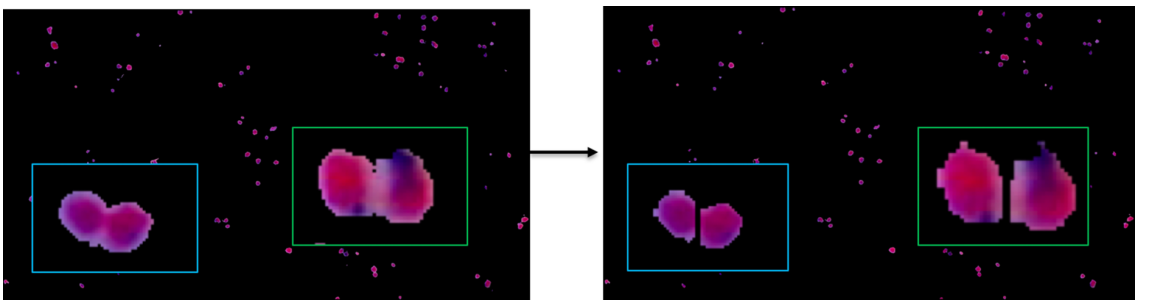

Fig. 7 Partitioning CEP17 signals.

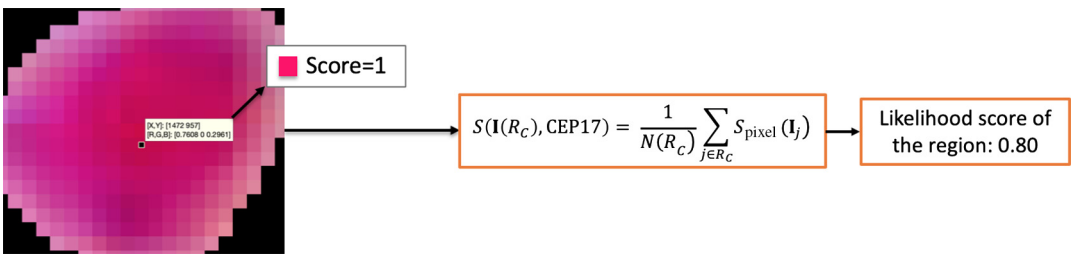

Fig. 8 Scoring a CEP17 signal.

The score for each pixel, $S_{\text{pixels}}(\mathbf{I})$, is defined as the probability that the color of the pixel is originated from the CEP17 signal. Then, the total likelihood score of the candidate region R_C for CEP17 signal is given as

$$S[\mathbf{I}(R_C), \text{CEP17}] = \frac{1}{N(R_C)} \sum_{j \in R_C} S_{\text{pixel}}(\mathbf{I}_j),$$

where $S_{\text{pixel}}(\mathbf{I}_j)$ denotes the score for each pixel calculated from RGB intensity $\mathbf{I}_j$, and $N(R_C)$ is the number of pixels in the region R_C. The details are presented in Sec. 7 Appendix B. Example of the score function for CEP17 is shown in Fig. 8. The proposed method selects a candidate as signal if the likelihood score is $\geq$0.80.

2.4 HER2 *Detection and Counting*

In CISH images, *HER2* signals appear as black, and the intensity varies from very dark to bright black. *HER2* signals also have intraslide or interslide size variation based on their biological signal within the nucleus. Moreover, the *HER2* probes may appear as a cluster of multiple *HER2* signals, and the size of the cluster varies as well. The proposed method consists of five steps for robust detection of *HER2* signals: (1) the background separation, (2) the removal of outliers, (3) separation of jointed signals, (4) scoring, and (5) counting signals in a cluster.

The first step of *HER2* detection is multilevel thresholding to separate background for *HER2* detection. Then, five-level thresholding is applied, and the pixels with intensity higher than the second lowest threshold are removed. This results in a base with *HER2* signals in the foreground to perform further operations for detecting *HER2*.

After the background separation, two types of outliers are removed. Originally, *HER2* signals appear as black, but the color changes when overlapped by magenta CEP17 dye or blue nuclei dye. Such pixels are considered as noise and eliminated by the proposed method. *HER2* pixels that are overlapped by magenta dye are eliminated by removing pixels with hue angle lies in-between 0 and 50 or 270 and 360 deg. Pixels with a hue angle between 150 and 250 deg are removed to eliminate pixels overlapped by the blue dye.

The next step is partitioning; jointed signals are partitioned using distance transformation and watershed. We assume that the size of *HER2* signals also follows a normal distribution, and signals within two standard deviations are considered, and region with a very small or large area is eliminated. We also estimated the maximum size of a single *HER2* signal from the distribution of individual *HER2* signals. This size is used as a dividing factor to count the number of individual signals in a *HER2* cluster. Usually, no watershed line with a different intensity compared to the signal basins in a *HER2* cluster exists, and thus the partitioning step cannot partition the clusters. We implemented an additional step to count individual signals in a cluster, which is the step (5). However, slightly jointed individual signals with a watershed line will be separated by the partitioning step.

Next, signals are scored using a similar technique to the CEP17, and then a candidate is selected if the likelihood score is $\geq$0.20, shown in Fig. 9.

Then, step (5) is implemented to count the number of signals in a cluster. Pathologists consider a small cluster as a collection of six *HER2* signals and a large cluster as a collection of 12 signals for the manual assessment, according to the VENTANA INFORM *HER2* dual ISH DNA Probe Cocktail Assay interpretation guide. Figure 10 shows the image of simulated *HER2* clusters.

Our method divides the cluster size by the factor to estimate the number of individual signals in the cluster. This factor is the maximum size of a single *HER2* signal, which is derived from the size distribution of individual *HER2* signals.

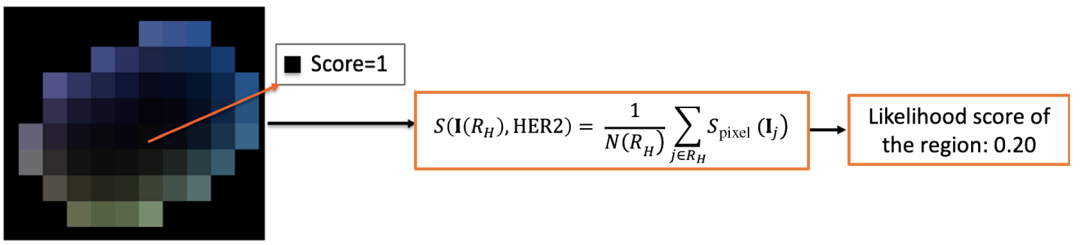

Fig. 9 Scoring an *HER2* signal.

Fig. 10 Simulated image of nuclei with *HER2* clusters: (a) large cluster and (b) small cluster.

2.5 *Signal Quantification*

The proposed method follows the ASCO/CAP 2018 guidelines to quantify the signals. CEP17 and *HER2* signals are counted for each nucleus. Then, nuclei are sorted based on the *HER2*-CEP17 differentiation value. Our target is to get the best representative nuclei to estimate *HER2* amplification, and the proposed method is designed to quantify those nuclei that exhibit at least two CEP17 and *HER2* signals, if available. The proposed method quantifies at least 20 nuclei with the highest *HER2*-CEP17 differentiation values. However, for some extremely positive cases, no nuclei with at least two CEP17 signals are present, and the proposed method selects nuclei with at least one CEP17 signal, as done by pathologists for the manual assessment. Furthermore, this method eliminates the nucleus with a low score value to ensure reliability. Next, the *HER2*/CEP17 ratio is calculated by dividing the total number of *HER2* with the total number CEP17 for the quantified nuclei. The average *HER2* copy number is calculated dividing the total *HER2* number by the number of quantified nuclei. Finally, the amplification status is determined based on the *HER2*/CEP17 ratio and the average *HER2* copy number. Figure 11 explains how signals are quantified and *HER2* status is determined. Another set of at least 20 nuclei is quantified similarly if IHC is 2+ for groups 2, 3, and 4 as shown in Fig. 11. In that case, the status is determined based on the *HER2*/CEP17 ratio and the average *HER2* copy number derived from at least 40 nuclei.

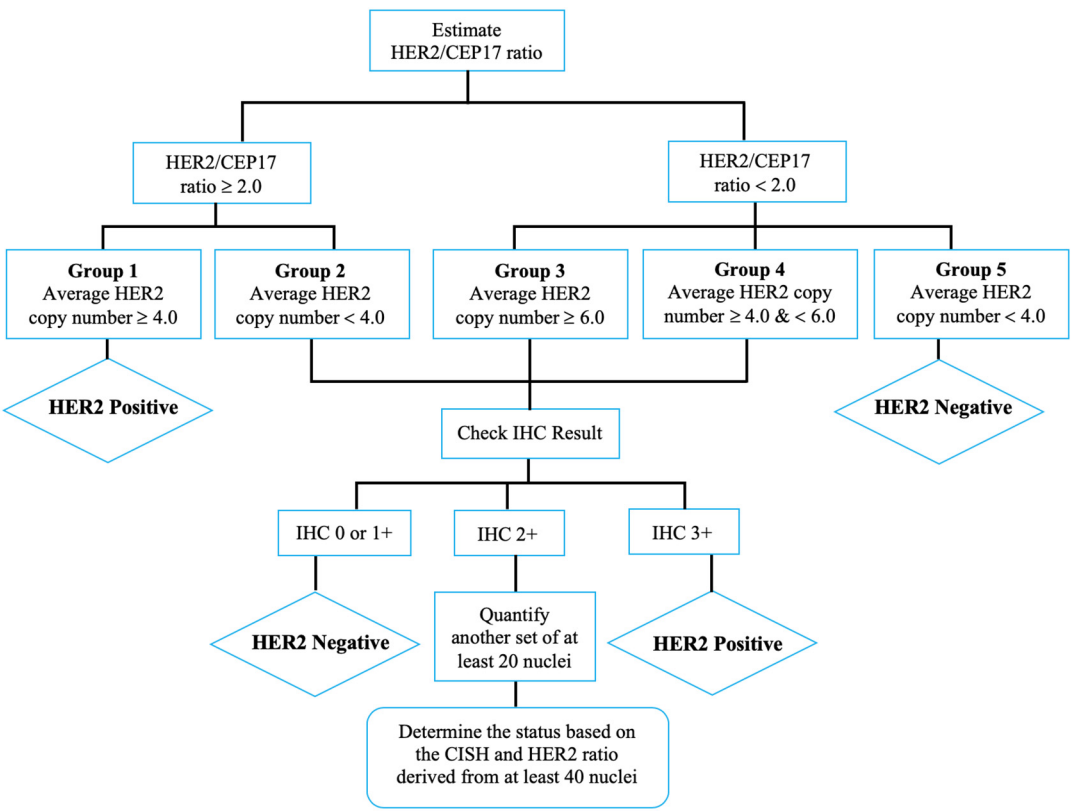

Fig. 11 Algorithm for signal quantification to determine the *HER2* status following the ASCO/CAP guidelines 2018.

3 Experiment Results

We developed an in-house application based on the proposed method for automatic quantification. Then, we quantified 22 BC specimens, selected randomly to include *HER2* negative, equivocal, and positive cases from the archives of Memorial Sloan Kettering Cancer Center, New York. Those patients were diagnosed with invasive BCs and tested with prior IHC, manual FISH, and manual CISH analysis. The cases were classified as positive, negative, and equivocal based on the IHC and manual FISH test results. The specimens were scanned by two different WSI scanners, 3DHISTECH P250 and 3DHISTECH P1000, to generate the WSIs that were evaluated by the proposed system. However, both of the scanners were equipped with an actual 40× objective lens (NA 0.95) and provided an image resolution of 0.13 μm/pixel. Thirteen specimens were scanned by P250 and nine specimens by the P1000 among the 22 slides at 40× magnification. Then, we quantified the 22 cases using the in-house application, and the results were compared with manual FISH and CISH analysis. The 22 cases included 10 *HER2* positive (amplified) and 12 negative (nonamplified) cases. The manual FISH and CISH counting of signals were performed by two pathologists as a team, and the assessment results reflect the consensus of them. Figure 12(a) shows the quantification result for a typical region of interest. We estimated the Pearson correlation coefficient between the *HER2*/CEP17 ratios of manual CISH and proposed automatic CISH quantification. We found a high concordance for both the *HER2*-positive and -negative cases. Furthermore, we calculated Cohen's kappa coefficient between the amplification status of manual and proposed CISH quantification.

3.1 *Nuclei Detection Result*

A nonlinear SVM binary classifier detects singular nuclei using the nine features that were selected using the sequential feature selection method. The SVM classifier was trained and tested using the 4-fold cross-validation. We extracted feature values from 6044 nuclei, which included 3341 positives and 2703 negatives. Then, 1511 nuclei are assigned randomly to each group, say A, B, C, and D. Each group contained at least 651 negatives and 782 positives. The dataset used for 4-fold cross-validation contained seven cases and was different from the dataset used for feature selection. The 6044 nuclei used for 4-fold validation were taken from 58 ROIs, which belonged to the seven cases. The average classification accuracy in 4-fold cross-validation was ~90%. Tables 2 and 3 show the results of the 4-fold cross-validation experiment. Furthermore, to ensure the validity of the nuclei detection method, we asked pathologists to identify

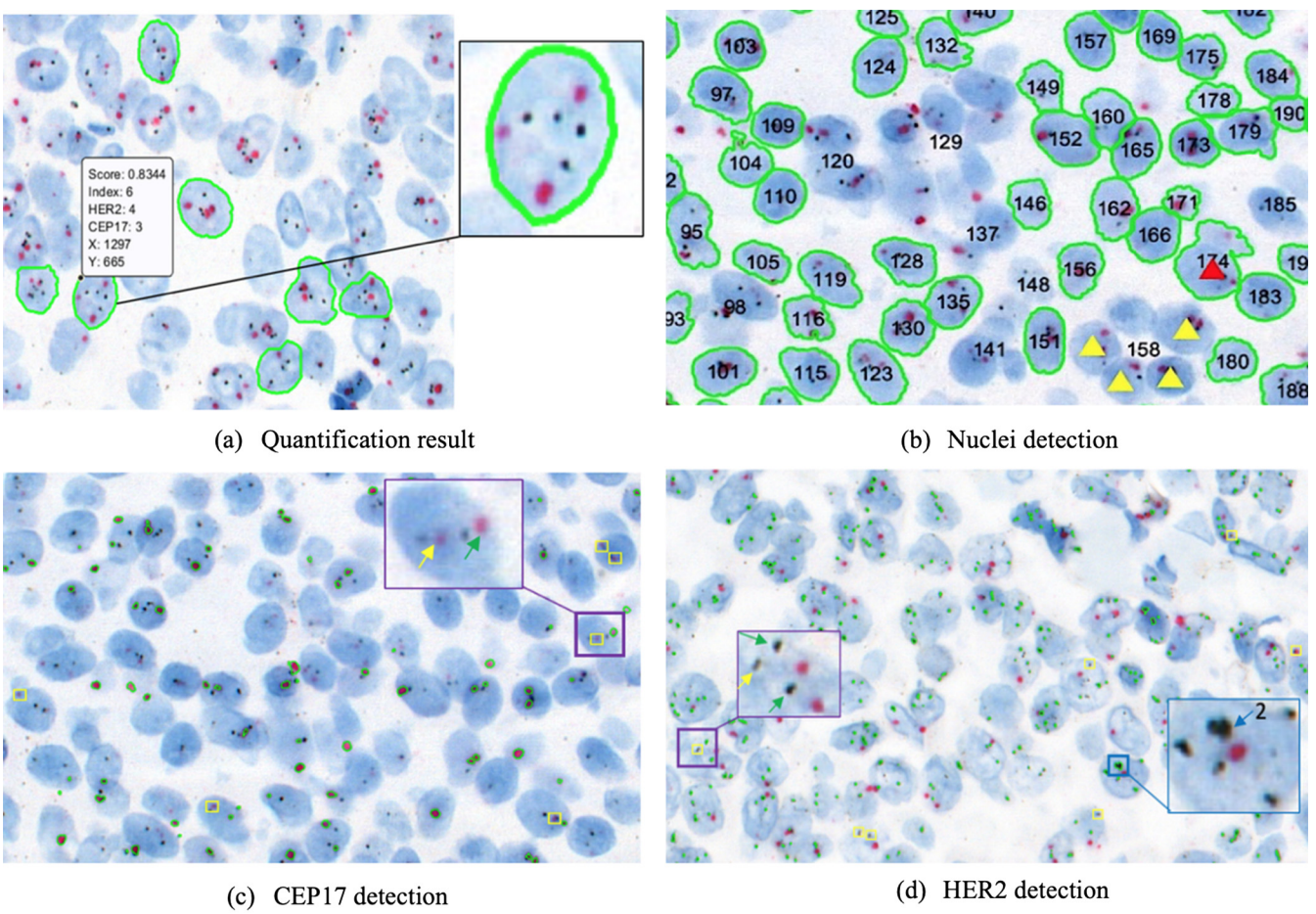

Fig. 12 (a)–(d) The results of proposed method. Example of quantification is shown in (a), (b) and (c), (d) Nuclei, CEP17, and *HER2* detection accordingly where the green boundary indicates the detection. Yellow and red triangles indicate undetected and false positives of singular nuclei in (a); green and yellow arrows indicate detected and undetected signal in (c) and (d) inside the magenta window. The blue arrow indicates a cluster of two *HER2* signals in blue window.

Table 2 4-fold cross-validation test result for singular nuclei selection.

	Training set	Testing set	TPR	SPC	ACC
Fold 1	B, C, D	A	0.9143	0.8875	0.9014
Fold 2	A, C, D	B	0.8889	0.9398	0.9113
Fold 3	A, B, D	C	0.8992	0.8997	0.8994
Fold 4	A, B, C	D	0.8894	0.8940	0.8914
Average			**0.898**	**0.905**	**0.900**

TPR, true-positive rate (sensitivity); SPC, true-negative rate (specificity); ACC, accuracy.

Table 3 Confusion matrix for singular nuclei selection using SVM in 4-fold cross-validation.

		Classifier prediction	
Total nuclei = 6044		Positive	Negative
Actual value	Positive	TP = 2999	FN = 342
	Negative	FP = 257	TN = 2446

Note: TP, true positive; FP, false positive; FN, false negative; TN, true negative.

false positives and false negatives. Pathologists selected seven representative regions of invasive cancer area, and the proposed method detected nuclei from the regions. Then, two pathologists individually identified the false detection and undetected singular nuclei for each region. Figure 12(b) shows the nuclei detection result for one of the representative regions. Representative regions were selected from seven different cases, four of them were scanned by P1000 and three by P250 3DHISTECH scanner. The dataset used for pathologists' evaluation is different from both: the dataset used for SVM 4-fold cross-validation experiment and the one that is used for feature selection. We performed the union of the pathologists' identification to calculate the total false positives and true negatives per region. Table 4 shows pathologists' evaluation for the nuclei detection. According to the ASCO/CAP guideline, the *HER2* status must be determined by quantifying at least 20 nuclei per case. The proposed method detects almost every singular nucleus from the annotated regions and quantifies the most representative ones. Table 4 shows that it detected 33 singular nuclei at lowest from a single region of a whole slide, which ensures that the method can detect enough nuclei to quantify at least 40 nuclei per whole slide if required.

3.2 *CEP17 Detection Result*

The proposed method detects the CEP17 and *HER2* signal with high accuracy. Figure 12(c) shows an example of CEP17 detection for a typical annotation where 210 signals were detected with no false positives but nine false negatives. To validate the accuracy of CEP17 detection, CEP17 signals were detected from the representative regions, and then pathologists identified

Table 4 Pathologists' evaluation for the nuclei detection.

SI	No. of nuclei detected	False positives	False negatives
1	166	4	3
2	106	1	4
3	81	0	2
4	67	2	3
5	33	0	4
6	33	1	1
7	37	0	2
Total	523	8	19

Table 5 Pathologists' evaluation for CEP17 detection.

SI	No. of CEP17 detected	False positives	False negatives
1	210	0	9
2	253	0	5
3	268	1	5
4	199	0	0
5	65	1	0
6	137	2	0
7	73	2	0
Total	1205	6	19

the false positives and false negatives. The method resulted in very few false positives and false negatives as shown in Table 5. The proposed method can detect CEP17 signals with high accuracy regardless of the color and size variations. All the 19 false negatives, shown in Table 5, were detected as candidates but eliminated from the selection due to the low score value. We eliminate weak signals to ensure the reliability of the quantification.

3.3 *HER2 Detection Result*

Figure 12(d) shows an example of *HER2* detection for the cropped area of representative regions where 560 signals were detected by the method, and pathologists identified nine false negatives. The false negatives were detected as candidates by the proposed method but eliminated due to the low score value. We performed a similar validation experiment such as the CEP17 detection using the seven representative images. Table 6 shows the *HER2* detection result by the proposed method with the false positives and false negatives, identified by the pathologists for the representative images.

Table 6 Pathologists' evaluation for HER2 detection.

Serial	No. of HER2 detected	False positives	False negatives
1	258	1	8
2	300	0	7
3	326	1	2
4	560	0	9
5	69	0	2
6	87	0	0
7	78	0	1
Total	1678	5	29

3.4 *Quantification Results*

The proposed method quantified 22 cases, and results were compared with the subspecialized breast pathologist's manual CISH quantification. The study was performed with Institutional Review Board (IRB) approval (IRB #17-287). Table 7 shows comparative results of *HER2* classification by manual FISH, manual CISH, and proposed CISH quantification method for 10 cases among the 22, and the IHC test results are provided as well. The proposed method has a Pearson correlation coefficient of 0.985 with manual CISH counting and 0.965 with manual FISH counting in terms of *HER2*/CEP17 ratio. The proposed method determined the *HER2* amplification status based on the *HER2*/CEP17 ratio and average *HER2* copy number per nuclei following the ASCO/CAP 2018 guideline. We estimated the correlation in terms of average *HER2* copy number and found a correlation of 0.885 with manual CISH and 0.92 with FISH. The FISH assessment was not performed for two cases among the 22, as the prior IHC test results were 3+, and the FISH test was not necessary according to the ASCO/CAP guidelines.

We confirmed the validity of the proposed method using the Bland–Altman plots; also, we estimated the p-values from the one-sided t-test. Figure 13 shows the Bland–Altman plots where the black line, orange line, purple line, and the shades represent bias (mean difference), the upper limit of agreement, the lower limit of agreement, and confidence intervals, accordingly. Figure 13(a) shows the comparison of the *HER2*/CEP17 ratio given by manual CISH analysis and the proposed method. The bias is 0.05 with 95% confidence interval −0.07 to 0.17, and the limit of agreement is −0.48 to 0.58. In the comparison with FISH, the bias is 0.08 with 95% confidence interval −0.12 to 0.29, and the limit of agreement is −0.78 to 0.95, as shown in Fig. 13(b). A small bias and narrow limit of agreement ensure the validity of the proposed method to quantify the *HER2* amplification. The p-value is 0.20 for the paired one-sided t-test, which is larger than 0.05 and shows the conformity between manual CISH and the proposed method. In the case of FISH, the p-value is 0.197. Further, we estimated the bias and limit of agreement in terms of *HER2* copy number. The bias is 0.67, and the limit of agreement is −2.55 to 3.9 with manual CISH while with FISH the bias is 0.41, and limit of agreement is −1.4 to 2.2.

In addition, we compared the proposed method with manual CISH and FISH using Cohen's kappa statistic in terms of *HER2* status and found 100% agreement in both cases.

4 Discussion

We developed an in-house application using the proposed method and enabled a system to quantify CISH WSI to determine the *HER2* amplification status automatically. The experimental results explained the feasibility of the method for *HER2* gene assessment. The proposed method allows access to more nuclei and then quantifies the representative ones, which

Table 7 Comparison of HER2 quantification and classification results.

		Manual FISH				Manual CISH				Proposed CISH			
SI	IHC status	Ratio	H/N	C/N	Status	Ratio	H/N	C/N	Status	Ratio	H/N	C/N	Status
1	2+	3.6	6.9	1.9	Pos	3.25	6.17	1.9	Pos	3.60	7.38	2.04	Pos
2	1 to 2+	1.4	2.6	1.9	Neg	1.41	2.87	2.02	Neg	1.40	2.80	2.00	Neg
3	2+	1.4	2.8	2	Neg	1.17	2.15	1.82	Neg	1.17	2.47	2.10	Neg
4	2+	6.6	14.6	2.1	Pos	6.39	12.1	1.9	Pos	6.62	8.34	1.26	Pos
5	N/A	2.3	5.8	2.6	Pos	2.29	5.85	2.55	Pos	2.31	6.00	2.59	Pos
6	1 to 2+	1.0	2.2	2.1	Neg	0.88	2.17	2.45	Neg	1.02	2.25	2.2	Neg
7	3+	N/A	N/A	N/A	N/A	4.63	12.8	2.77	Pos	4.13	11.2	2.72	Pos
8	1 to 2+	1.4	2.4	1.7	Neg	1.41	2.25	1.60	Neg	1.46	1.54	1.05	Neg
9	3+	2.6	7.0	2.7	Pos	2.71	6.85	2.53	Pos	2.76	7.40	2.68	Pos
10	2+	3.1	7.8	2.5	Pos	3.13	6.98	2.23	Pos	3.62	7.96	2.20	Pos

Note: Ratio, HER2/CEP17; H/N, HER2/nuclei; C/N, CEP17/nuclei; Pos, positive; Neg, negative; N/A, not available.

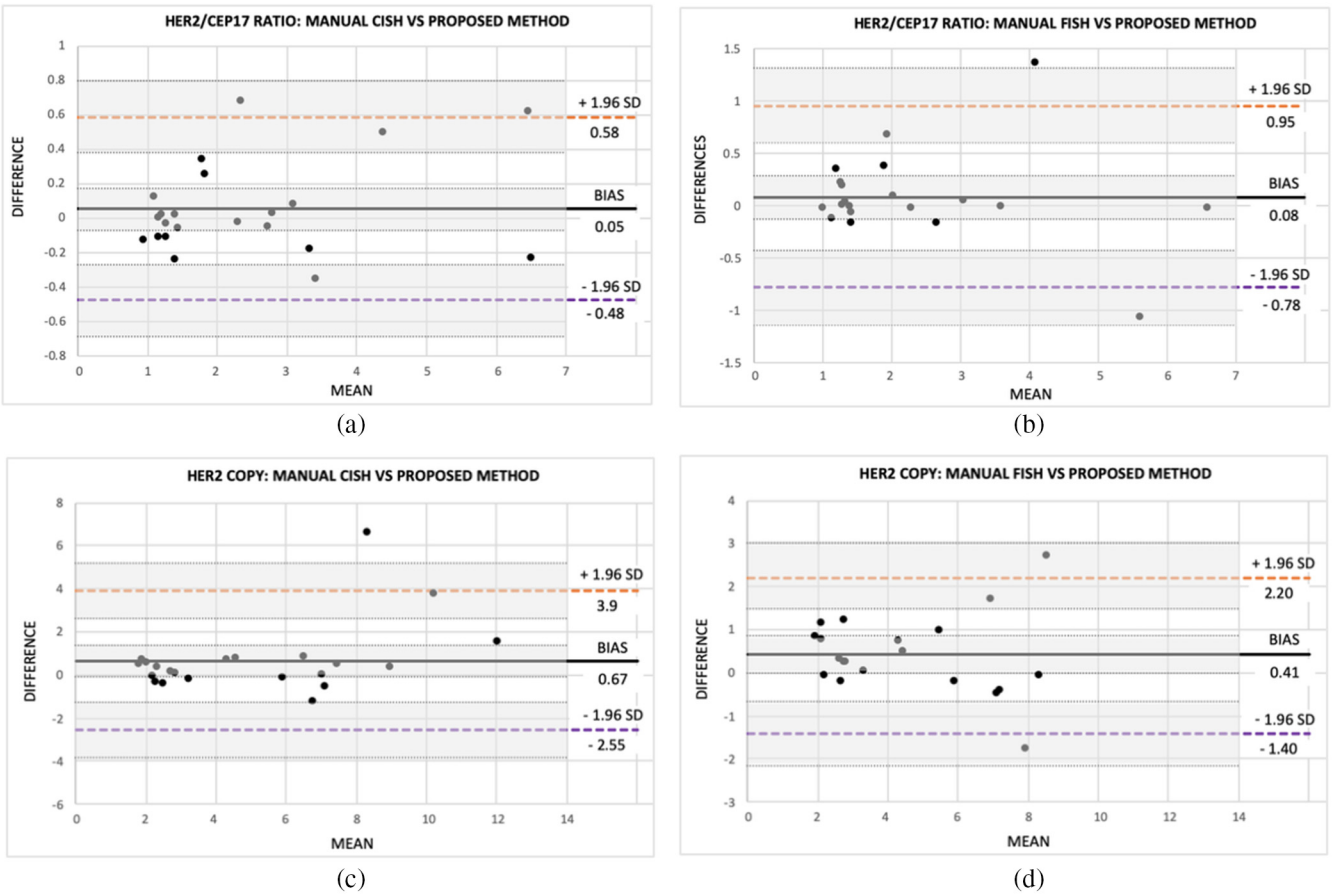

Fig. 13 (a)–(d) The evaluation of proposed method using Bland–Altman plots. (a), (b) The comparison of proposed method with manual CISH and FISH, accordingly in terms of *HER2*/CEP17 ratio. (c), (d) Same comparison in terms of *HER2* copy number per nuclei.

increases the reliability of the HER2 assessment. This system will significantly reduce the labor and time for HER2 assessment in hospitals and pathology departments. Moreover, it is a cost-effective approach compared to FISH. Currently, the application relies on pathologists for annotating the invasive tumor regions, and once the regions are annotated the proposed method performs the quantification. An invasive tumor detection method can be developed for automatic tumor annotation using machine learning such as a convolutional neural network. Then, the system will allow automatic tumor annotation followed by the automatic *HER2* assessment.

The image quality of the WSI is an important issue for the proposed quantification method. Out of focus images could affect the quantification results. In the future, the image quality of the annotated regions needs to be evaluated prior to quantification using the quality evaluation method.[18] In our experiment, slides were scanned by the WSI scanner at 40x magnification, which provided a 0.13-μm/pixel resolution.

The limitations of this work include the number of cases evaluated and the lack of reproducibility analysis. Only 22 cases were used to evaluate the proposed method, and the requirement exists to evaluate more before practical implementation. According to the CAP Accreditation Requirements for Validation of Laboratory Tests-2013, evaluating 40 cases for the clinical validation of the proposed system is a requirement.

Another limitation of the system presented in this paper is the ad-hoc approach to determine the parameters. Most of them were determined by observing the distribution of real data and referring statistical parameters such as the standard deviation. The expectation exists to remove or automatically optimize the ad-hoc parameters (i.e., thresholds for removing noises in CEP17 and *HER2* detection) in the future, but some of them need to be optimized for practical implementation.

We estimated the time requirements of the proposed quantification. The in-house application took 1 min on average to quantify an annotation. The turnaround time ranged from 3 to 20 min per case for the 22 cases. The time was estimated by using the application in a personal notebook with a 2.6-GHz Intel Core i5 processor without any external graphics card. Quantification time depends on many factors which include the following: the size of annotated regions, number of annotations, nuclei density, and image quality. Our target is to quantify a standard case within 1 min using the proposed method. In the future, further experiments are required to be performed to optimize the quantification time.

In the current situation, the manual FISH assay is used in practice but not by the breast pathologist as it requires long time and more effort. This paper presents the idea of the automatic CISH quantification system for HER2 assessment. This will allow the breast pathologists to perform HER2 assessments with less effort and time. Clinically, the FISH test is performed only for equivocal cases (IHC 2+), and one major reason is its cost. The proposed system can be used for all types of cases and to verify the IHC test results. In the future, the system should be

validated clinically following the CAP guidelines after optimizing the parameters and evaluating more cases.

5 Conclusion

The proposed automatic CISH quantification method demonstrates high concordance with the FDA-approved manual FISH and CISH counting for the 22 cases, and its potential for the real application is demonstrated.

6 Appendix A: Details of the Features Used for Nuclei Detection

Table 8 shows details of the 9 features used for nuclei detection which are selected from the 21 candidates using the sequential feature selection method.

7 Appendix B: Details of Scoring a CEP17 Candidate

We assume that the optical density of each pixel $\mathbf{g}$ is determined by the simple nonlinear model in Eq. (1), based on Beer–Lambert law. Figure 14 shows a typical candidate region R_C of CEP17 signal. The likelihood score is estimated for each pixel, say j inside R_C.

Then, in the CEP17 signal, the abundance a_C is supposed to be high, and a_b and a_H should be low. If we assume the abundance follows the normal and half-normal distribution and the pdfs of a_C, a_b, a_H are considered to be independent, i.e.,

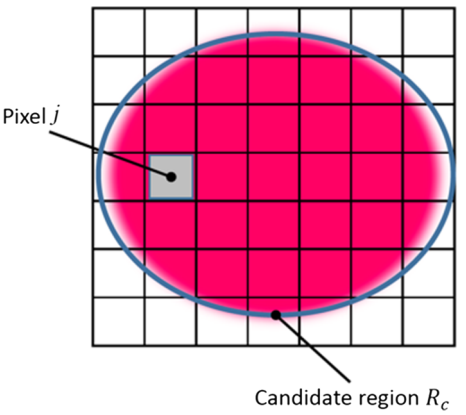

Fig. 14 Illustration of a candidate region for CEP17 scoring.

$$P(\mathbf{a}) = N(\boldsymbol{\mu}_a, \boldsymbol{\Sigma}_a),$$

where $a_C, a_b, a_H > 0$, $\boldsymbol{\mu}_a = (\mu_C\ 0\ 0)^t$, and $\boldsymbol{\Sigma}_a = \begin{pmatrix} \sigma_C & 0 & 0 \\ 0 & \sigma_b & 0 \\ 0 & 0 & \sigma_H \end{pmatrix}$.

Thus, if we consider a single pixel with the optical density $\mathbf{g}$, the likelihood of the pixel given CEP17 signal becomes

$$P(\mathbf{g}|\text{CEP17}) = \frac{1}{Z}\exp\left[-\frac{1}{2}(\mathbf{g}-\boldsymbol{\mu}_g)\Sigma_g^{-1}(\mathbf{g}-\boldsymbol{\mu}_g)^t\right], \quad (2)$$

Table 8 List of features used for nuclei selection.

Index	Features	Formula	Explanation
1	Roundness[14]	$\text{Roundness} = \frac{4\pi.\text{area}}{\text{Convex perimeter}^2}$	Ranges between 0 and 1 with one for perfect circle; insensitive to irregular boundaries
2	Area_to_peri[14]	$\text{Area\_to\_peri} = \frac{\text{Area}}{\text{Actual perimeter}}$	A higher value for well-shaped nuclei; sensitive to irregular boundaries
3	Std_cen_to_boundary[15]	$\text{std}_{\text{cen}_{\text{to}_{\text{boundary}}}} = \sqrt{\frac{\sum(\text{dist}-\overline{\text{dist}})^2}{n}}$ where dist is the distance from centroid to a boundary pixel for the nucleus and n is total number of pixels in the boundary	Std_cen_to_boundary is the standard deviation of distance from centroid to the boundary pixels. A higher value for irregularly shaped boundaries
4	Curl	$\text{Curl} = \frac{\text{length}}{\text{Fiber length}}$ where fiber length $= \frac{\text{perimeter} - \sqrt{\text{perimeter}^2 - 16.\text{area}}}{\text{Actual perimeter4}}$	Measures the desgree to which a nuclei is curled up. Higher curl value indicates lower curled up object
5	Elongation[14]	$\text{Elongation} = \frac{\text{Width}}{\text{Height}}$	It measures the aspect ratio. A higher value for well-shaped nuclei
6	Extent	$\text{Extent} = \frac{\text{Area}}{\text{Bounding box area}}$	The ratio of pixels inside the object to pixels inside the bounding box of object. A higher value of well-shaped nuclei
7	Solidity[14]	$\text{Solidity} = \frac{\text{Area}}{\text{Convex area}}$	Measures the density of an object. A higher value for well-shaped nuclei
8	Convexity[14]	$\text{Convexity} = \frac{\text{Convex perimeter}}{\text{Perimeter}}$	Measure the convexity of an object. A higher value for untruncated nuclei
9	Avg_bend_energy[16]	$\text{Avg}_{\text{bend}_{\text{energy}}} = \frac{\sum\text{curvature of each boundary pixel}^2}{\text{Total boundary pixels}}$	Measures the amount of bends in the boundary. A higher value for irregularly shaped boundaries

where $\boldsymbol{\mu}_g = \mu_C \mathbf{m}_C$, Z is a constant for normalization, and $\boldsymbol{\Sigma}_g = \mathbf{M}\boldsymbol{\Sigma}_C\mathbf{M}^t = \sigma_C \mathbf{m}_c \mathbf{m}_c^t + \sigma_N \mathbf{m}_N \mathbf{m}_N^t + \sigma_H \mathbf{m}_r \mathbf{m}_r^t$.

The log likelihood is given as

$$L(\mathbf{g}|\mathrm{CEP17}) = -(\mathbf{g} - \boldsymbol{\mu}_g)\Sigma_g^{-1}(\mathbf{g} - \boldsymbol{\mu}_g)^t = S_{\mathrm{pixel}}(\mathbf{I}),$$

where the constant term is omitted, and this is considered as the score of each pixel.

Based on the above concept, the score for a given pixel value $\mathbf{I}$, $S_{\mathrm{pixel}}(\mathbf{I})$ is calculated using a look-up table, which is derived as follows: first, a given RGB vector $\mathbf{I}$ is converted to $\mathbf{g}$ by log transform [Eq. (1)]. Next, the abundance vector $\mathbf{a}$ is estimated as $\hat{\mathbf{a}} = \mathbf{M}^{-1}\mathbf{g}$, but a negative value can occasionally appear in estimated $\hat{\mathbf{a}}$ because of some model error or noise. In such case, a negative to zero conversion is applied:

$$\tilde{a}_l = \begin{cases} \hat{a}_l & \text{if } \hat{a}_l > 0 \\ 0, & \text{otherwise} \end{cases},$$

where $l = C, N, r$. Then $\tilde{a} = (\tilde{a}_C\ \tilde{a}_N\ \tilde{a}_r)^t$, new $\tilde{\mathbf{g}}$ is obtained from converted $\tilde{a}_l$: $\tilde{\mathbf{g}} = \boldsymbol{M}^{-1}\tilde{\mathbf{a}}$. Finally, the score based on the log likelihood is obtained as

$$S_{\mathrm{pixels}}(\mathbf{I}) = L(\tilde{\mathbf{g}}|\mathrm{CEP17}) = -(\tilde{\mathbf{g}} - \boldsymbol{\mu}_g)\Sigma_g^{-1}(\tilde{\mathbf{g}} - \boldsymbol{\mu}_g)^t,$$

where $\boldsymbol{\mu}_g$ and $\boldsymbol{\Sigma}_g$ are estimated from the sample data of CEP17 in advance.

Disclosures

No potential conflict of interest was reported by the authors.

Acknowledgments

We are thankful to Kareem Ibrahim from Memorial Sloan Kettering Cancer Center and to Warren Alpert Foundation.

References

1. A. C. Wolff et al., "Guideline summary: American Society of Clinical Oncology/College of American Pathologists guideline recommendations for human epidermal growth factor receptor 2 testing in breast cancer," *J. Oncol. Pract.* **3**(1), 48–50 (2007).
2. A. C. Wolff et al., "Human epidermal growth factor receptor 2 testing in breast cancer: American Society of Clinical Oncology/College of American Pathologists clinical practice guideline focused update," *J. Clin. Oncol.* **36**(20), 2105–2122 (2018).
3. E. M. Van Der Logt et al., "Fully automated fluorescent in situ hybridization (FISH) staining and digital analysis of HER2 in breast cancer: a validation study," *PLoS One* **10**(4), e0123201 (2015).
4. H. Netten et al., "FISH and chips: automation of fluorescent dot counting in interphase cell nuclei," *Cytometry* **28**(1), 1–10 (1997).
5. E. Moerland et al., "Detection of HER2 amplification in breast carcinomas: comparison of multiplex ligation-dependent probe amplification (MLPA) and fluorescence in situ hybridization (FISH) combined with automated spot counting," *Cell. Oncol.* **28**(4), 151–159 (2006).
6. J. Konsti et al., "A public-domain image processing tool for automated quantification of fluorescence in situ hybridisation signals," *J. Clin. Pathol.* **61**(3), 278–282 (2008).
7. D. Furrer et al., "Validation of a new classifier for the automated analysis of the human epidermal growth factor receptor 2 (HER2) gene amplification in breast cancer specimens," *Diagn. Pathol.* **8**, 17 (2013).
8. G. Radziuviene et al., "Automated image analysis of HER2 fluorescence in situ hybridization to refine definitions of genetic heterogeneity in breast cancer tissue," *BioMed Res. Int.* **2017**, 1–11 (2017).
9. A. Sáez et al., "HER-2 gene amplification by chromogenic in situ hybridisation (CISH) compared with fluorescence in situ hybridisation (FISH) in breast cancer—a study of two hundred cases," *Breast* **15**(4), 519–527 (2006).
10. M. Tanner et al., "Chromogenic in situ hybridization: a practical alternative for fluorescence in situ hybridization to detect HER-2/neu oncogene amplification in archival breast cancer samples," *Am. J. Pathol.* **157**(5), 1467–1472 (2000).
11. A. C. Ruifrok and D. A. Johnston, "Quantification of histochemical staining by color deconvolution," *Anal. Quant. Cytol. Histol.* **23**(4), 291–299 (2001).
12. F. Keiko et al., "Development of support systems for pathology using spectral transmittance: the quantification method of stain conditions," *Proc. SPIE* **4684**, 1–8 (2002).
13. N. Reljin et al., "Multifractal-based nuclei segmentation in fish images," *Biomed. Microdevices* **19**(3), 67 (2017).
14. K. Win et al., "Detection and classification of overlapping cell nuclei in cytology effusion image using a double-strategy random forest," *Appl. Sci.* **8**(9), 1608 (2018).
15. C. Chang, S. Hwang, and D. Buehrer, "A shape recognition scheme based on relative distances of feature points from the centroid," *Pattern Recognit.* **24**(11), 1053–1063 (1991).
16. I. Young, J. Walker, and J. Bowie, "An analysis technique for biological shape," *Comput. Graphics Image Process.* **25**, 357–370 (1974).
17. J. Xie et al., "Two-stage hybrid feature selection algorithms for diagnosing erythemato-squamous diseases," *Health Inf. Sci. Syst.* **1**(1), 10 (2013).
18. M. S. Hossain et al., "Practical image quality evaluation for whole slide imaging scanner," *Proc. SPIE* **10711**, 107111S (2018).

Md. Shakhawat Hossain is a doctoral student at Tokyo Institute of Technology. Simultaneously, he is working as a graduate research assistant at Memorial Sloan Kettering Cancer Center. He earned a master's degree in information processing from the Tokyo Institute of Technology in 2017. His research roots in pathological image analysis.

Matthew G. Hanna is an assistant attending in breast pathology and informatics at Memorial Sloan Kettering Cancer Center, where he completed his oncologic pathology fellowship training. Prior appointments include being a clinical instructor of pathology informatics at the University of Pittsburgh, where he also completed his pathology informatics fellowship. He completed his residency training at the Mount Sinai Hospital in New York.

Naohiro Uraoka was a research fellow at the Department of Pathology, Memorial Sloan Kettering Cancer Center, and is currently a specially appointed assistant professor at Hiroshima University in Japan. He received his M.D. and Ph.D. from Hiroshima University. He is a board-certified pathologist of the Japanese Society of Pathology, and his research interests focus on information technologies and digital image analysis associated with surgical pathology.

Tomoya Nakamura is an assistant professor at Tokyo Institute of Technology. He received his PhD in information science from Osaka University in 2015. His current research interest is design of new computational imaging methodologies.

Marcia Edelweiss: Biography is not available.

Edi Brogi is the Director of Breast Pathology at Memorial Sloan-Kettering Cancer Center. She is also a professor of clinical pathology and laboratory medicine at the Weill Cornell Medical College. Her research activities focus on the diagnosis, study and treatment of breast diseases. Dr. Brogi was president of the International Society of Breast Pathology, 2017–19. She is an expert board member of the WHO book, *Classification of Breast Tumors* (5th ed.)

Meera R. Hameed is the Chief of Surgical Pathology Service at Memorial Sloan Kettering Cancer Center. She is a pathologist with expertise in bone and soft tissue and molecular pathology. She is also the co-director of the Warren Alpert Center for Digital and Computational Pathology at MSKCC. Her research involves exploring genomics and prognostic markers in rare tumors such as chordomas, osteosarcomas, and chondrosarcomas.

Masahiro Yamaguchi is a professor in the School of Engineering, Tokyo Institute of Technology. He received his D. Eng. from Tokyo Institute of Technology in 1994. Since 1989 he has been a faculty

member of the same institute, from 2011 to 2015 as a full professor at the Global Scientific Information and Computing Center. His research includes color and multispectral imaging, holography, and pathology image analysis. From 2011 to 2017, he was the chair of CIE TC8-07 "Multispectral Imaging."

Dara S. Ross is an assistant member of pathology at Memorial Sloan Kettering Cancer Center. She practices molecular and breast pathology. Her research interests include the assessment of HER2 amplification in solid tumors, with a focus in breast cancer, and genomic alterations relevant to the management and treatment of patients with breast cancer.

Yukako Yagi is the director of pathology digital imaging at Memorial Sloan Kettering Cancer Center. She received her Doctor of Medicine degree from Tokyo Medical University. She has a broad interest in various aspects of medical science, with a primary focus on the development of new technologies in digital imaging.